IL NUOVO CIMENTO **40 C** (2017) 200
DOI 10.1393/ncc/i2017-17200-9

COLLOQUIA: Physics in Collision 2017

Towards ϕ_3/γ extraction in a study of $D^*\rho$ at Belle

D. ČERVENKOV on behalf of the BELLE COLLABORATION

Institute of Particle and Nuclear Physics, Faculty of Mathematics and Physics, Charles University - V Holešovičkách 2, 180 00, Prague, Czechia

received 6 April 2018

Summary. — We report on progress in an angular time-dependent analysis of the $B^0 \to D^{*\mp}\rho^{\pm}$ decay at the Belle experiment. The study aims to establish a novel method for studying CP violation using this decay by measuring $2\phi_1 + \phi_3$ $(2\beta + \gamma)$ of the Unitarity Triangle.

1. – Introduction

The angle ϕ_3 of the standard CP violation Unitarity Triangle is the least well constrained of its angles. Its measurements are therefore of great interest to determine the validity of the Standard Model CP violation description.

This work describes a time-dependent angular CP violation analysis of the $B^0 \to D^{*\mp}\rho^{\pm}$ decay. The goal of this work is a world first measurement as neither Belle nor BaBar, or any of the other experiments, have published it before. This decay allows access to $2\phi_1 + \phi_3$ in a theoretically clean way, in contrast to similar decays such as $B^0 \to D^{*\mp}\pi^{\pm}$. In order to extract $2\phi_1 + \phi_3$ from the $B^0 \to D^{*\mp}\pi^{\pm}$ decay, one has to utilize certain external inputs, *i.e.*, assume $SU(3)$ symmetry between u, d and s quarks, and use results from related channels such as $B_s^0 \to D_s^{*\mp}\pi^{\pm}$. This method brings a hard-to-quantify theoretical uncertainty as well as experimental uncertainty from the related measurement itself. No such assumptions are necessary for $B^0 \to D^{*\mp}\rho^{\pm}$, thanks to its P $\to$ VV nature [1].

2. – P $\to$ VV decays

Considering that B^0 is a pseudoscalar meson and the fact that the overall spin projection on an arbitrary axis is a conserved quantity in a decay, we see that the spins of the daughter particles must be arranged in such a way that the resulting angular momentum projection $J_z = 0$. It is advantageous to consider the B meson center-of-mass system where the daughter particle momenta are back to back. Therefore, selecting the spin

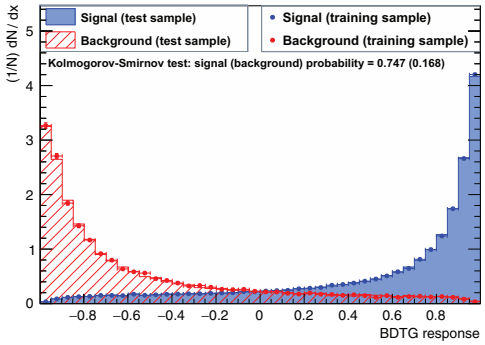

Fig. 1. – Continuum suppression BDT response.

projection axis to coincide with the momenta, no orbital momentum between the particles contributes to the J_z momentum projection. In other words, the spins of the two daughter particles must add up to zero J_z projection. Because of the choice of coordinate system, this means that the two daughter particles must have equal helicities.

In a P $\to$ PP decay both helicities are zero. In P $\to$ PV decays, the pseudoscalar has helicity zero, which forces the vector's helicity to be zero to satisfy the $J_z = 0$ condition. Thus in both cases there is just a single daughter helicity component of the wave function $|\Psi_f\rangle = |f_0\rangle$. In the case of VV decays, both daughters can have non-zero helicities, which results in three components satisfying $J_z = 0$, *i.e.*, $|\Psi_f\rangle = \sum_\lambda H_\lambda |f_\lambda\rangle$, where $\lambda \in \{+1, 0, -1\}$ is a helicity index. When squared to obtain physical observables, this sum gives rise to interference terms that preserve more information about $|f_\lambda\rangle$ then in the cases involving pseudoscalars, which allows to extract all the parameters from data.

3. – Continuum suppression

A significant part of the background in this analysis comes from $e^+e^- \to q\bar{q}$ processes, where $q \in \{u, d, s, c\}$ ($\sim$25000 events). We call this *continuum background*. It has different distributions of $\Delta E = E_B^* - E_{\rm beam}^*$ and $M_{\rm bc} = \sqrt{E_{\rm beam}^{*2} - \mathbf{p}_B^{*2}}$ as well as a different decay topology — it is jet-like as opposed to $e^+e^- \to B^0\bar{B}^0$ events. An effective way to suppress such background is combining topological and other variables in a multivariate discriminant. We use $M_{\rm bc}, \cos(\theta_{\rm thrust}), \cos(\theta_B)$ and 18 improved Fox-Wolfram moments [2] as inputs for a boosted decision tree (BDT). Using this method we achieve $\sim$4% signal loss and $\sim$70% background rejection. The distributions of BDT response for the signal and background training and testing samples are shown in fig. 1 together with an overtraining check based on a Kolmogorov-Smirnov test.

TABLE I. – *Selection efficiency and signal yield.*

Mode	Selection effeciency [%]	Signal yield
$K^\pm\pi^\mp$	13.5	17067 $\pm$ 218
$K^\pm\pi^\mp\pi^0$	4.9	21395 $\pm$ 257
$K^\pm\pi^\mp\pi^\mp\pi^\pm$	7.2	18102 $\pm$ 229
total	8.6	56564 $\pm$ 407

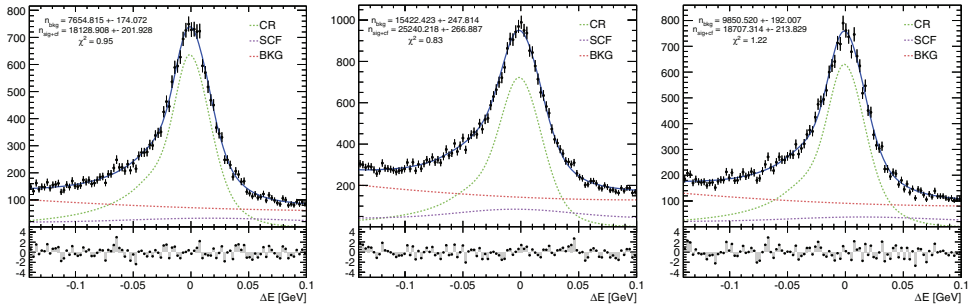

Fig. 2. – MC yield fits of $D^0 \to K\pi$ (left), $K\pi\pi^0$ (center) and $K\pi\pi\pi$ (right) modes.

4. – Signal yield

We reconstruct the $B^0 \to D^{*\mp}\rho^{\pm}$ channel with $\rho^{\pm} \to \pi^0\pi^{\pm}$ and $D^{*\mp} \to D^0\pi^{\mp}$. The D^0 is reconstructed from the three final states listed in table I, together with their selection efficiencies. The signal yield in each case is extracted from a one-dimensional fit to ΔE. To model the probability density functions (PDFs), we separate a large Monte Carlo simulated (MC) dataset, that corresponds to what is expected in data, into three different categories — correctly reconstructed signal (CR), self–cross-feed (SCF) and background (BKG). We define SCF as events with the signal decay present that are not correctly reconstructed, *e.g.*, a π used in the signal side reconstruction actually comes from the tag side. We fit each of the components separately and fix the PDF parameters from these MC fits. The fixed component PDFs then enter the final extended likelihood fit (see fig. 2) to an MC dataset containing CR, SCF and BKG, or actual data, from which we recover the number of signal and background events. Results from fits to MC datasets based on world average [3] branching fractions of our three signal modes are in table I.

5. – Transversity basis and cartesian coordinates

A particular choice of basis can significantly simplify the calculation of PDFs involved in angular analysis — for this reason we opt for the *transversity* basis. The helicity

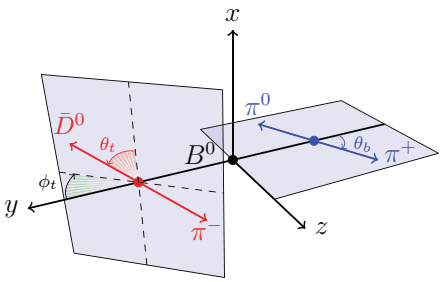

Fig. 3. – Transversity basis angles.

TABLE II. – *Time-dependent angular signal-only toy fit results.*

Variable	True	Fit	Error	Pull
$\|a_\parallel\|$	0.269	0.269	0.026	0.01
$\arg(a_\parallel)$	0.560	0.528	0.023	−1.40
$\|a_0\|$	0.941	0.940	0.009	−0.10
$\|a_\perp\|$	0.205	0.209	0.008	0.50
$\arg(a_\perp)$	3.110	3.110	0.013	−0.03
$x_\parallel$	0.008	0.118	0.040	2.78
x_0	0.005	0.084	0.014	5.61
$x_\perp$	0.008	0.086	0.028	2.75
$y_\parallel$	−0.007	−0.015	0.017	−0.53
y_0	−0.008	−0.010	0.005	−0.23
$y_\perp$	0.004	−0.024	0.024	−1.17
$\bar{x}_\parallel$	−0.010	−0.110	0.033	−3.02
$\bar{x}_0$	−0.008	−0.080	0.015	−4.81
$\bar{x}_\perp$	−0.006	−0.081	0.028	−2.72
$\bar{y}_\parallel$	0.002	0.001	0.021	−0.09
$\bar{y}_0$	0.005	0.001	0.005	−0.85
$\bar{y}_\perp$	−0.007	0.013	0.027	0.74

amplitudes H_λ are connected to the transversity amplitudes A_m in the following way:

$$A_\parallel = (H_+ + H_-)/\sqrt{2}, \tag{1a}$$

$$A_0 = H_0, \tag{1b}$$

$$A_\perp = (H_+ - H_-)/\sqrt{2}. \tag{1c}$$

The transversity angles are shown in fig. 3.

We introduce one more transformation — a switch from physical parameters to Cartesian coordinates. In principle we can extract

$$\rho_\lambda = r_\lambda e^{i(-2\phi_1-\phi_3+\delta_\lambda)}, \tag{2a}$$

$$\bar{\rho}_\lambda = r_\lambda e^{i(+2\phi_1+\phi_3+\delta_\lambda)}, \tag{2b}$$

where r_λ are the ratios of doubly Cabibbo-suppressed decays to Cabibbo-favored decays and δ_λ are strong phases. However, when r_λ are small, fitting can fail as $r = 0$ is a pole in the sensitivity of the other variables. To circumvent this, we switch $\{r_\lambda, \delta_\lambda, 2\phi_1 + \phi_3\} \to \{x_\lambda, y_\lambda, \bar{x}_\lambda, \bar{y}_\lambda\}$, with $\rho_\lambda = x_\lambda + iy_\lambda$ and $\bar{\rho}_\lambda = \bar{x}_\lambda + i\bar{y}_\lambda$. However, this introduces five new variables, hence a successive step has to be made to extract the physical parameters. We use a statistical method based on toy MCs to do this, which will be described in a separate article.

6. – Realistic MC fit results

We created a time-dependent angular maximum-likelihood fit that takes into account the detailed Belle detector simulation (acceptance, particle ID, etc.). We generated a realistic Belle MC signal sample with the following parameters:

- 60000 events,
- helicity amplitudes from CLEO [4],
- $r_\lambda = 1\%$,
- random values for strong phases:
  - $\delta_+ = -0.393$,
  - $\delta_0 = 0.785$,
  - $\delta_- = 1.571$,
- $2\phi_1 + \phi_3 = 1.794$ (value used in official Belle generic MC).

Fitting this MC sample we obtain the results shown in table II. In this fit we did not take realistic flavor tagging into account. After adding that, an increase of the uncertainties by $\sim 70\%$ is to be expected.

7. – Estimated sensitivity

We estimate the sensitivity that can be achieved from different datasets. These estimates are based on simpler (generator level) and more optimistic (slightly higher yield) toy MC, using robust $2\phi_1 + \phi_3$ extraction from x, y and adjusted for actual yield, resolution and flavor tagging. The resulting expected sensitivity for the weak angle is

- $\sigma(2\phi_1 + \phi_3) \approx 80^\circ$ (stat) for Belle,
- $\sigma(2\phi_1 + \phi_3) \approx 11^\circ$ (stat) for Belle II at 50 ab^{-1}.

This is *without any external input*. We can choose to decrease $\sigma(2\phi_1 + \phi_3)$ in exchange for giving up this "external independence". One way to do that is by taking r_λ from other measurements such as $B_s^0 \to D_s^{*\mp}\rho^\pm$.

8. – Conclusion

We have presented the first time-dependent angular analysis to determine $2\phi_1 + \phi_3$ using the $B^0 \to D^{*\mp}\rho^\pm$ decay. We have reported on the current progress as well as estimates of statistical uncertainties with current and future Belle/Belle II datasets.

REFERENCES

[1] London D., Sinha N. and Sinha R., *Phys. Rev. Lett.*, **85** (2000) 1807.
[2] Bevan A. J. *et al.*, *Eur. Phys. J. C*, **74** (2014) 3026.
[3] Olive K. A. *et al.*, *Chin. Phys. C*, **38** (2014) 090001.
[4] Csorna S. E. *et al.*, *Phys. Rev. D*, **67** (2003) 112002.